InSb ARRAYS WITH CCD READOUT FOR 1.0- TO 5.5-μm INFRARED APPLICATIONS*

J. D. Phillips, J. B. Scorso, and R. D. Thom
Santa Barbara Research Center
Goleta, California

ABSTRACT

The application of charge-coupled device (CCD) readout and signal processing techniques to infrared (IR) arrays is leading to a new generation of IR focal plane assemblies with significant improvements in performance. In this paper, two approaches for fabricating indium antimonide (InSb) arrays with CCD readout are discussed. The hybrid approach integrates InSb detectors and silicon CCDs in a modular assembly via an advanced interconnection technology. In the monolithic approach, the InSb infrared detectors and the CCD readout are integrated on the same InSb chip. Both approaches utilize intrinsic (band-to-band) photodetection with the attendant advantages over extrinsic detectors. The status of each of these detector readout concepts, with pertinent performance characteristics, is presented.

I. INTRODUCTION

The development of high-density two-dimensional IR focal plane arrays (FPAs) has been pursued extensively in recent years. The use of CCD readout and signal processing techniques has made possible the combination of detection and multiplexing functions on the focal plane with an attendant reduction in sensor power, size, and weight. Further, enhanced sensitivity can be obtained, if required, by implementing the time delay and integration (TDI) function in the CCD readout registers. The resulting IR array assemblies are ideally suited to, for example, earth resource and outer planet IR imaging applications.

Two distinct methods can be used to achieve IR detection on the focal plane — intrinsic and extrinsic photodetection. The extrinsic approach uses appropriately doped silicon, thus allowing device fabrication on silicon chips. The intrinsic mode of detection, however, utilizes band-to-band photodetection which provides significant operating advantages over the extrinsic approach. In particular, higher operating temperatures ($\simeq$ 77° to 100°K) are possible with intrinsic detectors as opposed to 50°K or less for extrinsic detector arrays. Further, the larger absorption coefficient of intrinsic materials provides not only higher quantum efficiencies but lower crosstalk between detector sites than is feasible for extrinsic detectors. The result is a decided systems advantage for intrinsic detectors.

Two concepts for implementing the advantages of intrinsic detectors are discussed in this paper for the case of InSb detectors. The hybrid concept utilizes an advanced interconnection technology to combine the maturity of silicon CCD technology with an array of backside-illuminated InSb photodetectors. The interconnection procedure for this approach is discussed in Section II along with performance data for the InSb detector arrays.

The alternate concept is a complete monolithic structure in which the IR detection and CCD signal readout functions are incorporated on the same InSb chip. This approach obviously eliminates the requirement of an interconnection technology, but it suffers from the relative lack of maturity in the processing of metal-insulator semiconductor (MIS) structures on intrinsic IR detector materials, for example InSb. A viable MIS process has been developed in this laboratory for InSb, and CCDs have been successfully operated. Four-element and 20-element imaging arrays have been designed with fabrication and testing of these devices proceeding at this time. The status of this CCD program will be discussed in Section III.

The possibility of achieving TDI in real time, within the imaging device itself, is an attractive feature of both the monolithic and hybrid InSb/CCD arrays which can significantly increase sensor signal-to-noise ratio (SNR). In Section IV, this performance improvement is illustrated by considering a future generation Landsat Sensor with a monolithic InSb TDI CCD 16 × 16 array operating at 95°K. A four-fold increase in detectivity over a conventional InSb detector array with discrete current-mode preamplifiers is estimated for the particular configuration and spectral bands considered.

II. HYBRID InSb ARRAYS

The demonstration of a 32-element solder bump interconnected FPA was the beginning of hybrid FPA development. Building on this initial success, significant advances in the interconnection technology have been made. In particular, a process was developed in 1974 by which InSb diode detectors could be solder bump connected to silicon CCDs, the resulting structure thinned and then illuminated from the back side. A schematic of such a structure (the BInSb structure) is shown in Figure 1.

The thinning of the back surface of the structure, to a thickness of a few μm, is necessary to achieve photoresponse in the InSb material. Since the silicon CCD readout circuitry is located below

*This work supported in part by NASA under Contracts NAS1-13937 and NAS1-14395.

the InSb in this device, a BInSb array can have virtually all the available FPA area photosensitive; i.e., a high filling factor is feasible. Taking advantage of this property, a 32 × 32 element backside-illuminated array is currently being fabricated. With 1024 detectors located on 0.1-mm (0.004-inch) centers, the device has a filling factor of 95%.

To ascertain the performance characteristics of backside-illuminated arrays, photovoltaic (PV) InSb detectors were assembled to silicon test substrates having metallized lead patterns. A primary measure of the array performance is the quantum efficiency (η) of the structure using backside-illuminated geometry. The quantum efficiency depends on the InSb thickness, the wavelength of incident radiation, and the intrinsic InSb properties. In particular, InSb possesses a high optical absorption coefficient (α) since it is an intrinsic IR detector. As a result, most incident radiation will be absorbed within a few μm of the back surface. The minority carriers (holes for p-on-n InSb diodes considered here) generated by this absorption must then diffuse through the InSb bulk to the diode depletion region. At this point, the carriers result in photocurrent in the usual manner. The importance of the diffusion process to the overall detector quantum efficiency is thus significant.

The process is governed by the continuity equation for minority carrier transport subject to the appropriate boundary conditions at the back surface and at the p-n junction depletion region edge. With this equation, a model using known material parameters has been found to predict the quantum efficiency of BInSb detectors. A curve based on this model is shown in Figure 2 where calculated values of η are shown versus substrate thickness. Two data points are also shown in the figure for different substrate thicknesses. The agreement with the model predictions is observed to be good.

The surface recombination velocity (s) at the back surface is also a critical property which can strongly affect the η, particularly at shorter wavelengths. If s is high ($>> 10^3$ cm/sec), then the majority of the photogenerated holes will recombine at the back surface with a corresponding decrease in quantum efficiency. To ensure a low back surface s value, a passivation process has been developed which yields, repeatedly, detectors with the ideal response of Figure 3. The quantum efficiency is observed to be $\eta \simeq 0.6$ and uniform across the response region of InSb. As noted, the uniformity at the shorter wavelengths demonstrates the success of the passivation process for low s structures.

Finally, the detectivity (D*) and responsivity (R_λ) of the BInSb structure are observed to be comparable to conventional InSb detectors. This point is illustrated by Figure 4 where these parameters are plotted for a BInSb array. It is clear from the figure that the structure is operating at close to BLIP (background limited performance) limit.

III. MONOLITHIC InSb CCD ARRAYS

Charge-coupled devices have been fabricated on InSb substrates and successfully operated. This success has prompted the design of full monolithic InSb arrays which combine InSb MIS detectors with InSb CCDs for signal readout. These arrays are now being fabricated and tested. Due to the importance of these developments for focal plane imagery, it is of interest to examine the status of InSb CCDs in some detail.

The devices fabricated thus far are four-phase (4ϕ) p-channel overlapping gate structures with six basic layers. A cross-sectional view of the device structure is shown in Figure 5. It is clear from the figure that the structure is conventional with the possible exception of the channel stop metal. This layer, used in lieu of the channel stop diffusion of silicon CCD structures, defines the active channel regions of the CCD. Note that the presence of this metal adds one additional layer to the CCD structure, thus complicating the topography of the device. The primary metal used in device fabrication is titanium with silicon monoxide (SiO) being the prime insulator. Typical dimensions of the device include 0.1 μm for the metals, 0.15 μm for the gate insulator, and 0.3 μm for the buried metal insulator.

The first device fabricated in this fashion utilized conservative design rules, due to the initial unknowns of InSb MIS processing, so that the CCD gate lengths were approximately 50 μm. It was a 4-bit device and was successfully operated early in 1975 at a clock frequency of 5 kHz. The proper 4-bit delay was observed using 4ϕ clocking, and the observed charge transfer efficiency (CTE) per transfer was 0.90.

This low CTE value is due primarily to the 50-μm gate lengths in the CCD register, and a shorter gate length device ($\simeq$ 25 μm) was designed. The new design includes a 2-bit 4ϕ CCD shift register and a 9-bit 4ϕ CCD with four InSb MIS detectors. A recently fabricated chip is shown in Figure 6. This four-element imager incorporates a transfer gate with the MIS detectors to control access of integrated signal charge into the CCD register. The result is a completely monolithic, albeit small, InSb imager. Already in fabrication with testing of some devices in progress, the successful demonstration of charge transfer from the MIS detectors into the CCD registers is expected shortly.

The 2-bit device has been successfully operated at a clock frequency of 10 kHz, again using 4ϕ operation of the device. The requisite 2-bit delay in the device output is shown in Figure 7 for the case of (a) a single charge packet, and (b) a pulse train

of six charge packets being electrically injected into the CCD register. The CTE can be obtained directly from this figure. Thus, for the single charge packet case, the magnitudes of the first and second output pulses (A and B, respectively) are related to the CTE by

$$N(1 - CTE) = N\epsilon = B/A \qquad (1)$$

where N is the number of transfers of the packet and ϵ is the transfer inefficiency of the device. Since one of a pair of output gates in the 2-bit structure was clocked in this operation, a value of N = 9 is appropriate in the present case. Using this result in equation (1) with the measured A and B values from Figure 7, the result is

$$\epsilon \cong 0.0214 \text{ or } CTE \simeq 0.978$$

A similar result is obtained using the pulse magnitudes of the multiple input pulse train. For this type of input, however, a different relationship between N, ϵ, and the pulse magnitudes must be used.

The expected improvement in the CTE due to the decreased gate length is shown in Table 1. This table was obtained by applying the charge control theory for CCDs as developed by Lee and Heller.[1] The basic assumptions of this model are that (a) the effects of interface states in the CCD can be treated by using an effective time constant (τ_s) for all states, and (b) that charge redistributes instantaneously during the transfer period of CCD operation. The τ_s value was obtained by fitting the CTE of the 50-μm gate length device to the Lee and Heller model. The resulting τ_s, 5 μsec, was then assumed to be valid for the shorter gate length devices and CTE values were computed on this basis.

It is evident that an additional parameter entering the model is the storage well depth of the CCD. The depth appropriate to the 25-μm structure is 1 volt, and for this value the projected CTE is 0.983. This CTE evidently compares favorably with the observed CTE of 0.978. It may thus be concluded that the projected CTE values for still shorter gate length devices are also accurate. Indeed, the tabulated values are the minimum CTE values expected since (a) no fringe field coupling, which increases with shorter gate lengths, is included in the analysis for Table 1, and (b) the continuing improvements in InSb MIS processing are expected to further increase the operating CCD well depth.

Due to these factors, both a 20-element imager with 13-μm gate lengths and a 2-element imager with 10-μm gate lengths are currently being processed along with the 25-μm 4-element imagers. From Table 1, the CTE for these structures should approach 0.999 with existing technology. Since programs to improve the InSb CCD processing sequence and interface state properties are in progress, the final CTE values obtained will be even higher. Some applications are possible even with CTE values of 0.995, however, and it is reasonable to consider a particular application configured around InSb CCD imagers on the focal plane.

IV. MONOLITHIC InSb CCD ARRAY FOR AN EARTH RESOURCES SENSOR

Several applications exist in the fields of remote earth sensing and planetary exploration for which the use of InSb CCD monolithic focal plane arrays with TDI would increase system performance. A partial list of potential applications includes forest fire surveillance and mapping, atmosphere temperature sounding in the 4.3-μm CO_2 band, pollution monitoring, mineral exploration and other geological uses, and distinguishing between clouds and water surfaces, all of which present mid-IR (1 to 5 μm) signatures. To estimate a representative level of performance improvement that should be realized with these arrays, a future generation Landsat Sensor has been considered using a monolithic InSb TDI CCD focal plane, and its performance has been calculated.

Such a future Landsat Sensor configuration is shown in Figure 8. This sensor system utilizes (intrinsic) silicon detectors on a warm focal plane for reflected light bands and one or more InSb TDI CCD arrays on a cold (95°K) focal plane for mid-IR bands. Other arrays may also be included on the cold focal plane for long-wavelength IR bands.

The Landsat spacecraft is assumed to be positioned in a sun-synchronous orbit at 705 km altitude. The IFOV of the system is 42 μrad giving a ground resolution of 30 meters, an improvement of a factor of 2.5 over the present multispectral scanner systems (MSS) now in orbit. A scan mirror (Figure 8) scans the linear arrays in the perpendicular-to-track direction to produce a 185 km swath width. This scan motion allows on-focal-plane TDI to be readily implemented without changing the basic sensor configuration.

The focal plane organization for the InSb TDI CCD array is shown in Figure 9. The number of detectors in TDI is 16; thus, the array is 16 × 16 or 256 elements total. The selection of a 16-element TDI subarray is not necessarily optimum; for this choice, the subarray detectivity in the ideal case is $\sqrt{16} = 4$ times the individual detector D*. Since the performance improvement is proportional to the square root of subarray length, relatively small gains are achieved by using numbers of detectors greater than about 30. The 16 subarrays are aligned with the perpendicular-to-track direction and staggered as shown in Figure 9 to provide contiguous coverage in the along-track direction.

The InSb CCD array parameters and the system parameters assumed for the future Landsat Sensor are given in Table 2. The two spectral bands

considered are a 1.55- to 1.75-μm band and a 3.6- to 4.1-μm (atmospheric window) band. Detectors are 0.05-mm (0.002-inch) square for the 42-μrad IFOV and telescope parameters assumed. The InSb CCD parameters are listed in the lower half of Table 2. These are based on typical design values and measured material parameters and represent presently achieved values or those predicted for the near future. Because of the relatively low backgrounds and scene radiances in these spectral bands and system dwell time, the CCD bit area required is not large, nor is it necessary to taper the CCD register in this case as needed in some TDI applications. This results in the compact array configuration shown in Figure 9.

Using these parameters, the results of D* calculations for the two spectral bands are given in Table 3. In each spectral band, detectivity is calculated for: (a) a conventional system configuration with a 16-element linear array (i.e., one detector/IFOV in the perpendicular-to-track direction); and (b) the 16 × 16 InSb TDI CCD array. The conventional system utilizes PV InSb detectors and current-mode preamplifiers. Noise and D* for this array were calculated using the usual noise current formalism. For the InSb TDI CCD, detectivity was calculated based on noise variance estimates for detector, CCD, and output circuit sources as tabulated in the second and fourth columns of Table 3.

In both bands, the InSb TDI CCD is shown to offer a significant detectivity improvement. For the conventional detector array, D* is amplifier/feedback resistance noise limited in both bands. In the 3.6- to 4.1-μm band, for example, D* is about 45% of the BLIP value for the PV InSb discrete amplifier case. For 16 elements in TDI, the ideal BLIP D* is four times higher. The estimated InSb TDI CCD D* in the 3.6- to 4.1-μm band is, with all noise variances considered, about 50% of this limit. Effective performance in this band is improved by a factor of 4 through use of the monolithic InSb TDI array.

In the 1.55- to 1.75-μm band, thermal background radiation is negligible and reflected sunlight dominates scene radiance. It is instructive to examine the improvement in system SNR in this band when InSb TDI CCDs are used. The minimum radiance N_{min} in this band is approximately 80 μw/cm^2-sr. Using a clear aperture area for the telescope equal to 85% of the primary mirror area and other optical parameters in Table 2, this radiance results in a power 7.8×10^{-11} watts, or 6.5×10^8 photons/sec, imaged on each detector. The summed signal charge at the TDI CCD output is $16 \times 0.75 \times 6.5 \times 10^8 \times 4.5$ μsec $= 3.5 \times 10^4$ charges. Including shot noise in signal, the total noise electron count is 604 electrons, yielding SNR = 58 at the minimum radiance level. For the single detector case, using R = 1 a/w, the noise current in Table 3, and including signal shot noise, the corresponding SNR at N_{min} is 19. These calculations illustrate the potential impact of InSb CCD arrays on future spacecraft sensor systems.

V. CONCLUSIONS

Two approaches to combine intrinsic IR detection and signal readout on the focal plane have been discussed. Hybrid arrays using InSb PV detectors solder bumped to silicon CCDs and backside illuminated have been successfully fabricated. The resulting structure exhibits uniform quantum efficiency ($\eta = 0.6$) and BLIP performance throughout the InSb response region.

Charge-coupled devices with 50-μm and 25-μm gate lengths have been fabricated directly on InSb and successfully operated. The observed charge transfer efficiencies (CTE) of 0.90 and 0.978, respectively, are in agreement with theoretical predictions for these gate lengths. Projected CTE values of 0.999 are expected for shorter gate length structures now being fabricated and tested. Among these structures is a 20-element imager with 13-μm gate lengths which completely integrates IR detection and CCD readout on the same InSb chip. An infrared system configured around the InSb CCD monolithic concept has been presented. A factor of 4 improvement over conventional detectors in system performance is predicted.

ACKNOWLEDGMENTS

The authors would like to thank J. H. Beeler and M. E. Dugger for the fabrication and characterization of the device structures reported in this paper.

REFERENCE

1. Lee, H. S., and Heller, L. G., "Charge-Control Method of Charge-Coupled Device Transfer Analysis," IEEE Trans. on Electron Devices, Vol. ED-19, 1270 (1972).

Table 1. Calculated Transfer Efficiency Versus Gate Length for InSb CCD

GATE LENGTH (μm)	WELL DEPTH (volts)	INTERFACE STATE LOSS	EFFICIENCY (CTE)
50	0.5	9.36×10^{-2}	0.90 (0.90)
25	1.0	1.65×10^{-2}	0.983 (0.978)
13	2.0	2.51×10^{-3}	0.997
10	2.0	1.61×10^{-3}	0.998
7.5	2.0	9.11×10^{-4}	0.999

f_C = 5 kHz; $\tau_S = 5 \times 10^{-6}$ sec; NO FRINGE FIELD; 4Φ CLOCK MODE

Table 2. InSb CCD Array Parameters and Representative System Parameters for Future Landsat Sensor

SYSTEM	InSb SPECTRAL BANDS		1.55 TO 1.75 μm 3.6 TO 4.1 μm
	ORBIT ALTITUDE		705 km
	ORBITAL PERIOD		98.5 minutes
	IFOV		42 μrad
	CROSSTRACK SWATH		0.26 rad
	f/NO.		f/3
	FOCAL LENGTH		1.2 meters
	OPTICAL EFFICIENCY		0.5
	DETECTOR AREA	A_D	2.58×10^{-5} cm^2
	SAMPLE RATE		1/RFOV
	FOCAL PLANE TEMPERATURE	T	95°K
	NO. OF DETECTORS PARALLEL-TO-TRACK		16
DETECTOR/ CCD	QUANTUM EFFICIENCY	η	0.75
	CCD BITS/DETECTOR		1
	BIT LENGTH		56 μm
	BIT AREA	A_B	1.42×10^{-5} cm^2
	THIN OXIDE CAPACITANCE		4×10^{-8} f/cm^2
	CLOCK VOLTAGE		5 volts
	DARK CURRENT (95°K)	J_D	10 μa/cm^2
	INTERFACE STATE DENSITY	N_{SS}	10^{11}/cm^2-eV
	INPUT/OUTPUT CAPACITANCE	(C_{IN}, C_O)	0.5 pF
	OUTPUT DEVICE NOISE AT 1 Hz	V_1	12.5 μV/$\sqrt{\text{Hz}}$

Table 3. Detectivity Calculations for Conventional and InSb TDI CCD Arrays

		SPECTRAL BAND (μm)			
		1.55 TO 1.75		3.6 TO 4.1	
RESPONSIVITY (a/w)	R	1.0		2.3	
BACKGROUND PHOTON FLUX (photons/sec cm^2)	Q_B	NEGLIGIBLE		7.4×10^{13}	
NUMBER OF DETECTORS PERPENDICULAR-TO-TRACK	N	1*	16**	1*	16**
SCAN EFFICIENCY		0.8	0.4	0.8	0.4
IFOV DWELL TIME (μsec)		9.0	4.5	9.0	4.5
BANDWIDTH (kHz)	Δf	55	110	55	110
CLOCK FREQUENCY (kHz)	f_c	---	220	---	220
DETECTOR TYPE		PV InSb	InSb CCD WITH PHOTOGATES	PV InSb	InSb CCD WITH PHOTOGATES
PREAMPLIFIER		CURRENT-MODE	NONE	CURRENT-MODE	NONE
DETECTOR DYNAMIC IMPEDANCE (Ω)		6×10^8	---	6×10^8	---
SHORT CIRCUIT CURRENT (a)		NEGLIGIBLE	---	2.3×10^{-10}	---
FEEDBACK RESISTANCE (Ω)		2×10^7	---	2×10^7	---
EXCESS NOISE CURRENT (a/$\sqrt{\text{Hz}}$)		3×10^{-15}	---	3×10^{-15}	---
TOTAL NOISE (a/$\sqrt{\text{Hz}}$)		1.7×10^{-14}	---	1.9×10^{-14}	---
NOISE ELECTRONS:					
PHOTON	N_P	---	NEGLIGIBLE	---	321
RESET	N_{RST}	---	130	---	130
DARK	N_D	---	385	---	385
FAT ZERO	N_{FZ}	---	130	---	130
INTERFACE STATE	N_{FIS}	---	358	---	358
OUTPUT DEVICE	N_{OUT}	---	140	---	140
TOTAL	N_T	---	574	---	658
D^*_λ (cm Hz$^{\frac{1}{2}}$/watt)		3.0×10^{11}	1.3×10^{12}	6.2×10^{11}	2.7×10^{12}
D^*_{BLIP} (η = 0.75)		---	---	1.4×10^{12}	5.5×10^{12}

$$N_P^2 = N\eta Q_B A_D T_C \qquad N_{FIS}^2 = 0.69 \frac{kT}{q} A_{CCD} N_{SS}$$

$$N_{RST}^2 = 2kTC_O/3q^2 \qquad N_{OUT}^2 = (V_1 C_O/q)^2 / n(1/T_C)$$

$$N_D^2 = \left[\frac{NJ_D T_C}{q}(A_D + \tfrac{1}{2}A_B)\right] \qquad D^*_\lambda = \left(\frac{A_D T_C}{2}\right)^{\frac{1}{2}} \frac{N\eta\lambda}{hcN_T}$$

$$N_{FZ}^2 = 2kTC_{IN}/3q^2$$

*CONVENTIONAL SYSTEM **TDI CCD

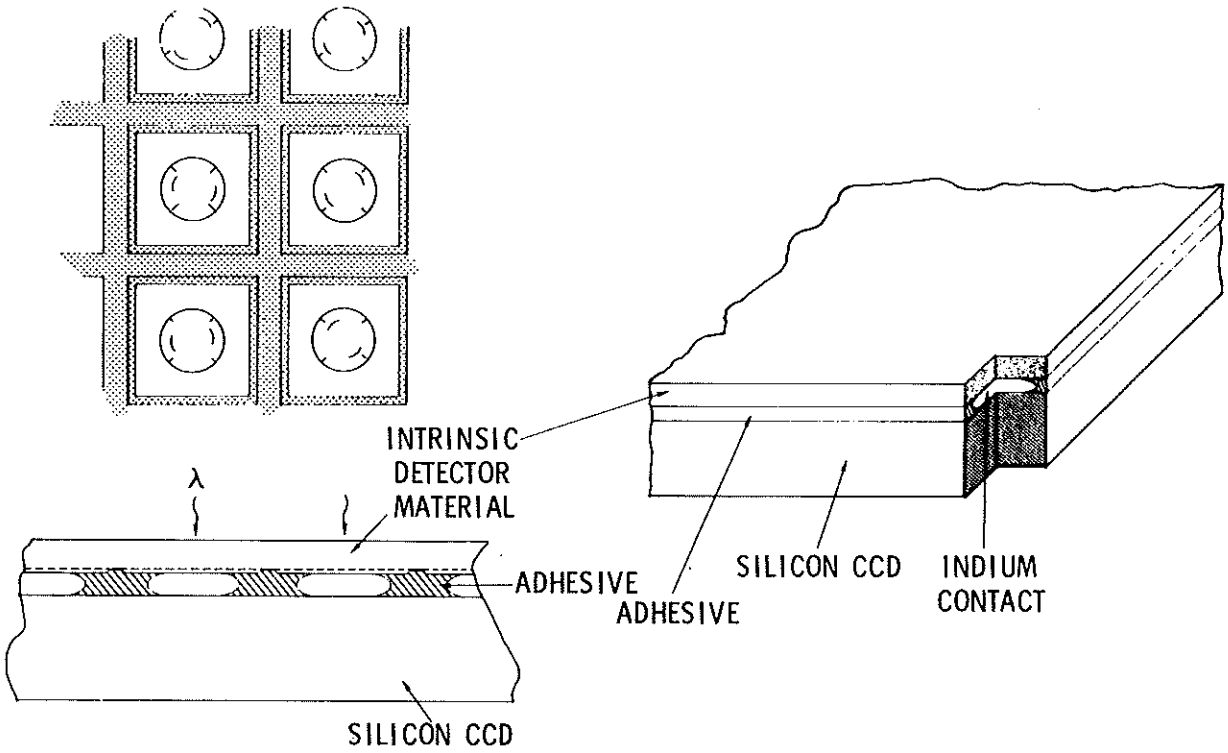

Figure 1. Schematic of Backside-Illuminated InSb Structure

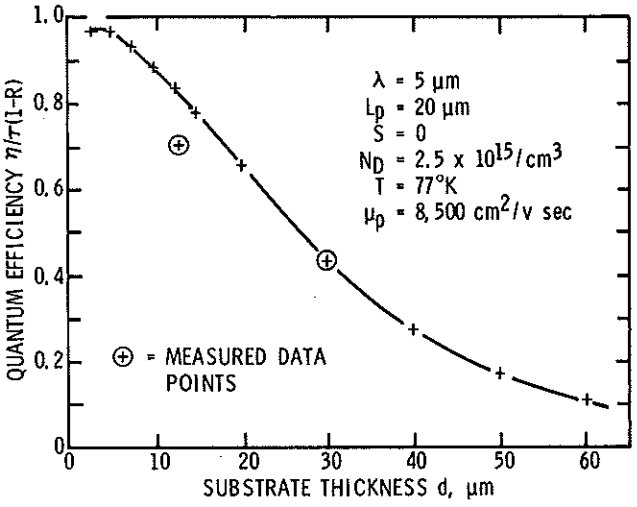

Figure 2. Quantum Efficiency Versus Substrate Thickness of Backside-Illuminated InSb (BInSb) Detectors

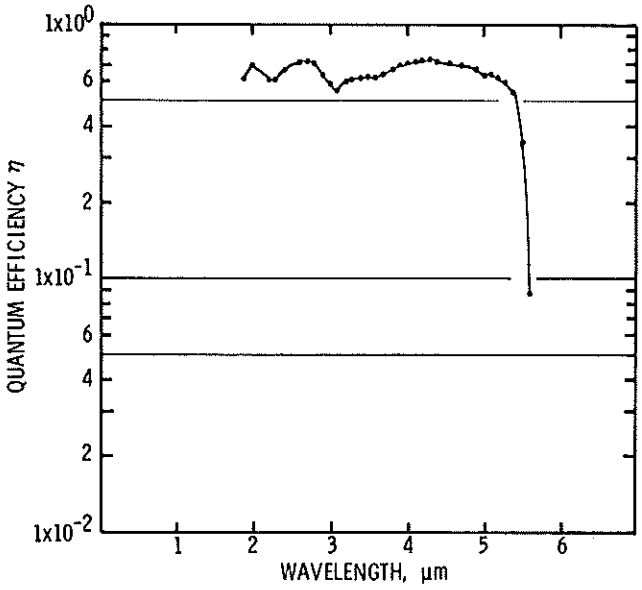

Figure 3. Measured Quantum Efficiency Versus Wavelength for Backside-Illuminated InSb (BInSb) Detectors

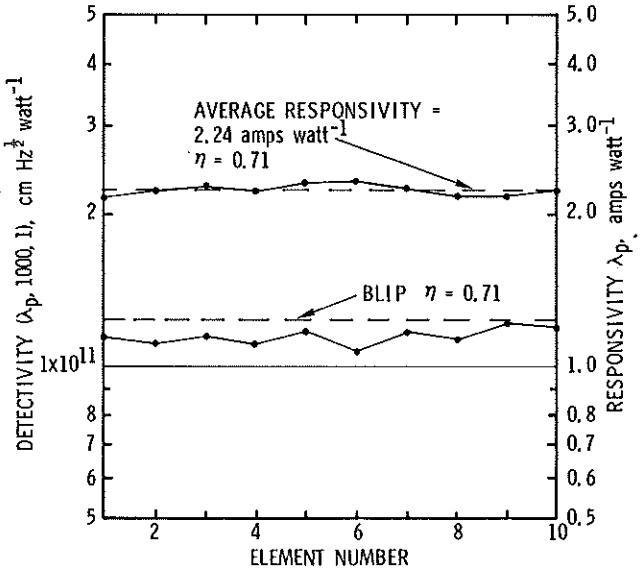

Figure 4. Performance Data on a Recently Measured Backside-Illuminated InSb (BInSb) Array ($Q_B = 1 \times 10^{16}$ photons/sec-cm^2; T = 77°K)

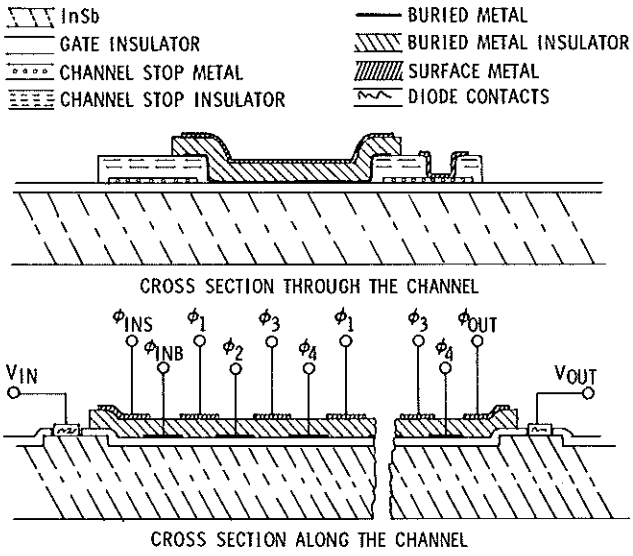

Figure 5. Cross-Sectional View of 4ϕ Overlapping Gate CCD

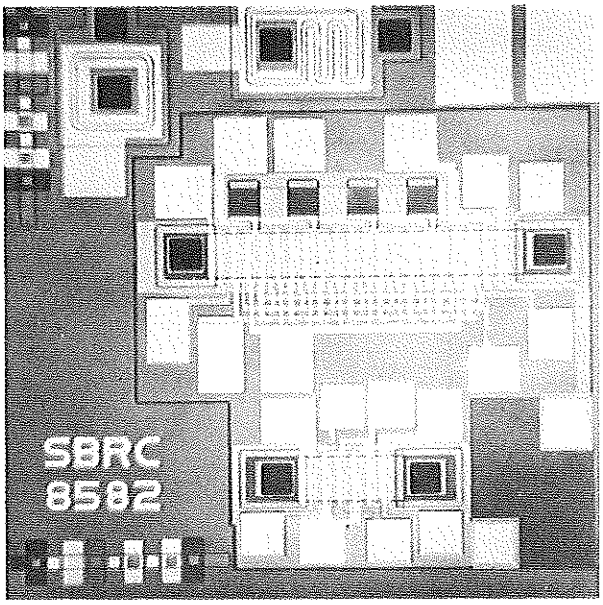

Figure 6. InSb CCD Test Chip with 9-Bit Linear Imager and 2-Bit CCD

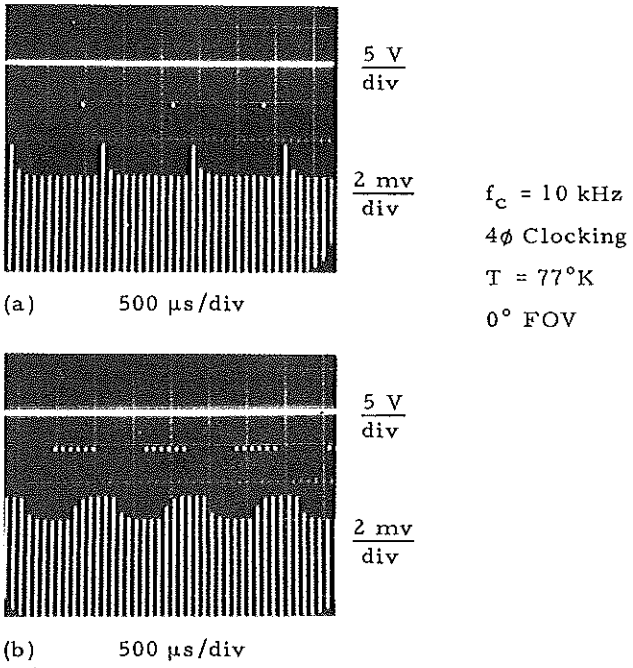

Figure 7. InSb CCD Output Waveform Two-Bit, 4ϕ CCD

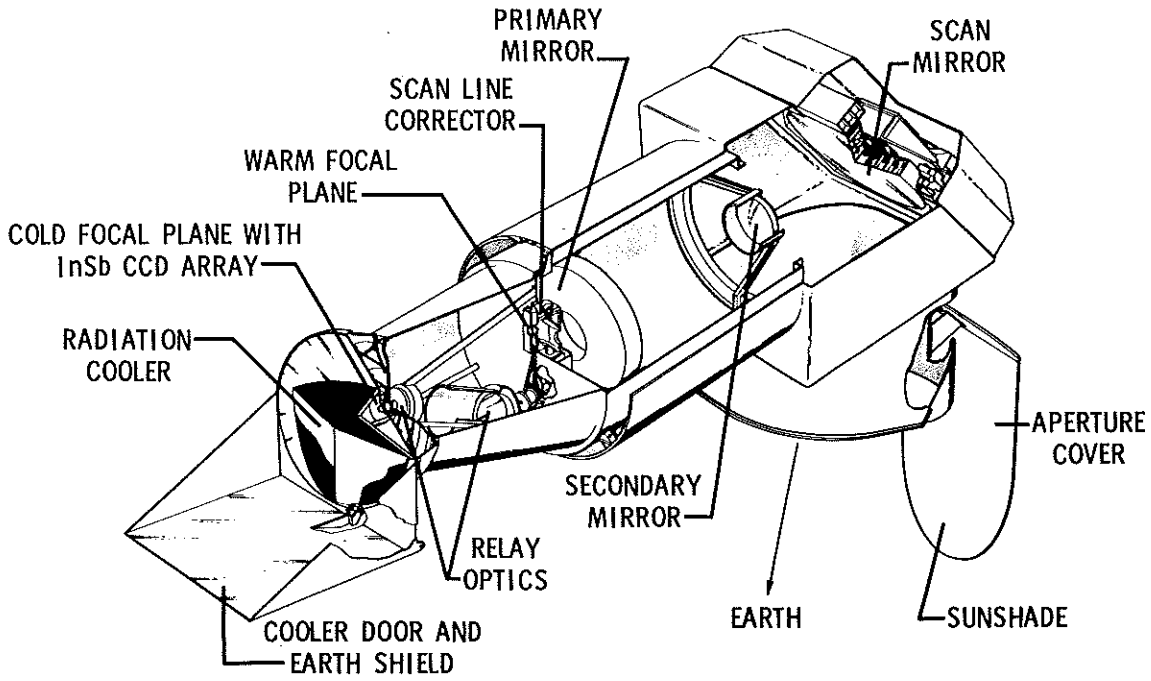

Figure 8. Future Generation Landsat Sensor with InSb CCD Focal Plane

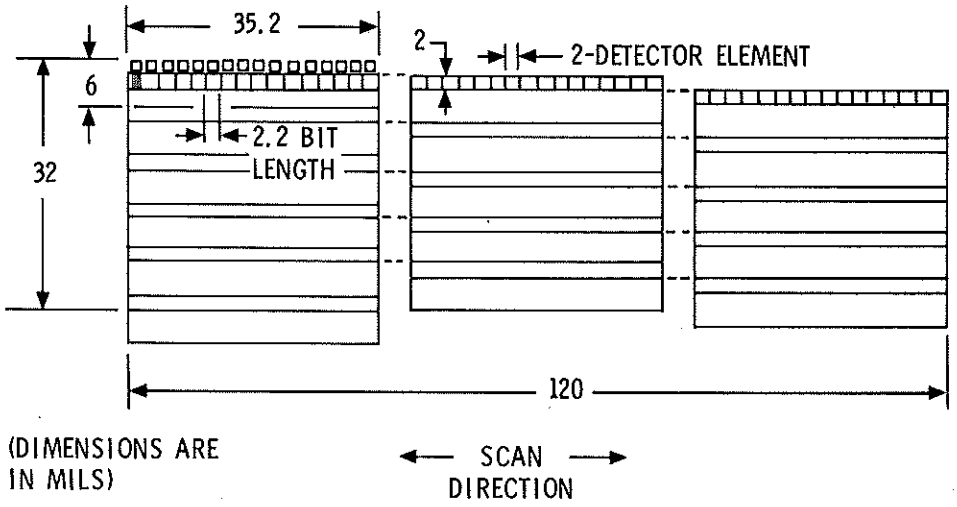

Figure 9. Focal Plane Organization for 16 × 16 InSb TDI CCD Array